



## **Experimental determination of methane dissolution from simulated subsurface oil leakages**

**Wilson Sauthoff, University of California Santa Cruz**

*Mentors: Peter G. Brewer, Edward T. Peltzer, Peter M. Walz*

*Summer 2013*

**Keywords: Raman spectroscopy; dissolved gases; saturated oil; methane; carbon transport**  
**ABSTRACT**

Subsurface oil leakages and increased offshore drilling efforts have raised concern over the fate of hydrocarbon mixtures of oil and gas in ocean environments. Recent wellhead, pipeline, and riser failures in the Gulf of Mexico are extreme examples of this problem. Understanding the mechanism and rate of vertical transport of hydrocarbon chemical species is necessary to predict the environmental impact of subsurface leakages. In a series of controlled experiments, we carried out a deep-sea field experiment in Monterey Canyon to investigate the behavior of a gas-saturated liquid hydrocarbon mass rising from the seafloor. Aboard the RV *Rachel Carson*, we used the ROV *Ventana* to transport a laboratory prepared volume of decane ( $C_{10}H_{22}$ ) saturated with methane gas ( $CH_4$ ) to mimic a subsurface seafloor discharge. We released the oil and gas mixture into a vertically oriented open bottom cylindrical glass tube (4.844 cm diameter) followed by methane loss rate measurements both at discrete depths, and during rapid, continuous vehicle ascent from 800 to 100 m water depth to monitor changes in dissolution and bubble nucleation. Using laser Raman techniques and HD video we quantified the chemical state of the hydrocarbon fluid, including rate of methane gas dissolution. The primary methane Raman peak was readily observable within the decane C-H stretching complex. Variation in the amount of gas dissolved in the oil greatly influences oil plume density and in turn oil plume vertical rise rate. Our results show that the rise rate of the hydrocarbon mass significantly exceeds the rate at which the excess methane was lost by dissolution. This result

implies that vertical transport of methane in the saturated hydrocarbon liquid phase can greatly exceed a gas bubble plume ascending the water column from a seafloor source. These results and observations may be applicable to improved understanding of the composition, distribution, and environmental fate of leaked hydrocarbon mixtures.

## INTRODUCTION

Subsurface hydrocarbon leaks of oil and gas mixtures, both human-induced and natural, pose potential harm to benthic, pelagic, and epipelagic marine environments. Solubility and volatilization of hydrocarbon species determines oil and gas mixture transport, marine bioavailability, and atmospheric contributions. To date, most oil spills to date have occurred at the ocean surface (e.g. liquid oil from *Exxon Valdez*) or shallow water (e.g. 1969 Santa Barbara blowout). However, the increasing number of offshore drilling operations (National Research Council, 2003), threats from predicted increase in storm surge strength (IPCC 2007), and the recent Deepwater Horizon oil spill (Kemsley 2013) have made evident the need to examine subsurface oil and gas mixture leaks. Understanding the solubility characteristics of these hydrocarbon species underpins understanding the fate and consequences of leaked hydrocarbon mixtures at depth.

An explosion and fire destroying the Deepwater Horizon oil platform occurred on April 20, 2010 (Ryerson et al., 2011). Below the oil platform, a massive subsurface leak of pressurized oil and gas ensued from the BP Macondo wellhead (1520 m depth; 80 km offshore). The ensuing subsurface leak lasted over three months and leaked 4.9 million of barrels of oil and gas mixture into the Gulf of Mexico. Initial studies have focused on quantifying leak rate (Crone and Tolstoy, 2010) and dispersion (Adcroft et al., 2010; Mezić et al., 2010) using water column measurements. However, water column studies fail to capture aromatic hydrocarbon species that rapidly evaporate at the sea surface (National Research Council, 2003). Only 20% of the leaked mixture was either recovered via the wellhead or surface skimming and a mere 5% burned, leaving the majority (75%) to reside in the ocean environment (McNutt et al., 2012). Unrecovered subsurface leaked oil has one of four fates: dissolution into seawater, evaporation into atmosphere, adhering to coastal areas, or seafloor settlement. The vast majority of unrecovered oil dissolved into the water column to form vertical or horizontal deep plumes of mixed oil, gas, hydrate, and seawater (Ryerson et al., 2011; Paris et al., 2012). Such a plume will

continue to ascend in the water column or remain buoyant as long as dissolved gases remain in the oil. Dissolution of methane or other gases will reduce buoyancy of a plume. Studies of oxygen consumption by microbial respiration show that subsurface oil plumes can create localized areas prolonged oxygen depletion when methane oxidation is present (Adcroft et al., 2010). Oxygen depletion could potentially resemble (in volume and severity) the 'dead zone' in the Gulf of Mexico (Kessler et al., 2012). Microbial conversion of leaked hydrocarbons results in the production of carbon dioxide (CO<sub>2</sub>) resulting in localized acidification. Acidification can have biological ramifications at depth (e.g. undersaturation of aragonite). Another point of concern with deep oil plumes is the inability to ameliorate spilled oil via skimming or burning with surface oil slicks. There is also the potential for a delayed resurfacing of deep oil plumes in locations remote from the original spill.

A 'ground-zero' sample of the leaked oil and gas mixture from the BP Macondo wellhead before mixing with surrounding seawater was collected by researchers at Woods Hole Oceanographic Institution (Kemsley 2013). This sample was used a 'fingerprint' of the oil pollution from the site at locations far removed from the wellhead. Separation experiments elucidated the partitioning and chemical evolution of contained hydrocarbon species. Understanding the proportions of contained hydrocarbon compounds facilitated improved quantification of spilled oil volume. Analyses of the unmixed wellhead oil yield the mixture as being 74% saturated hydrocarbons, 16% aromatic hydrocarbons, and 10% polar hydrocarbons, with methane being the most prevalent species at 80 mole % (McNutt et al., 2012).

Methane (CH<sub>4</sub>) is a hydrocarbon species of particular interest due to its potent global warming potential at 21 times the global warming potential of one carbon dioxide molecule (10<sup>2</sup> year timescale; Lelievre et al., 1998). Similar to rising atmospheric carbon dioxide levels, methane is also on the rise with a current concentration more than double preindustrial level (750 to 1,730 ppbv; Cicerone and Oremland, 1988; Lelievre et al., 1998). A better working knowledge of the mechanism and rate of vertical oceanic transport of methane will enhance our understanding of both natural and anthropogenic methane sources. Numerous naturally occurring methane seep sites have been discovered by visual (Dando et al., 1994) and acoustic studies (Paull et al., 1995). Additionally vast stores of methane hydrate along continental margins present a potential positive feedback warming mechanism as warmer ocean temperatures perturb the hydrate stability zone such that large methane pools are released (Buffett, 2000; Milkov,

2004). Additionally human activities contribute to atmospheric methane concentrations by perturbing subsurface geological methane pools.

Methane is produced in sediments and anaerobic waters. Large pools of methane exist in the form of methane hydrate or in the saturated state in deep sea oil reservoirs. Methane may reach the surface mixed layer and eventually the atmosphere by rising bubbles or turbulent diffusion (Joyce and Jewell, 2003). Turbulent transport is the primary transport pathway in deep water. Although vertical transport of methane via bubble ebullition is not the primary transport mechanism, this process is a growing concern (Leifer and Patro, 2002). Many parameterizations control bubble rise velocity and mass transfer including bubble size, temperature (Leifer et al., 2000), surfactants (Vasconcelos et al., 2003), and rise velocity (Leifer and Patro, 2002). Some of these parameters are highly variable in ocean environments and others are not well established. It has been observed that a large mass fraction of a methane bubble dissolves into surrounding seawater during vertical ascent (McGinnis et al., 2006).

McGinnis et al. use the example of an 11 mm diameter bubble released at 90 m depth would maintain an 11 mm diameter when it reached the sea surface but with only ~5% of initial mass based on experimental data of Rehder et al. (2002). Most of the mass transfer occurs at deeper depths near the seafloor where methane bubbles nucleate resulting in higher dissolved methane concentrations closer to the hydrocarbon leakage source (McGinnis et al., 2006). Methane readily dissolves into seawater. When methane is dissolved in seawater, vertical transport is only possibly by turbulent diffusion. That is methane bubbles do not transport sizable amounts of methane to the mixed surface layer or atmosphere from deep water sources. Methane transport by way of saturation in oil plumes is an alternate mode of reaching the mixed surface layer and eventually the atmosphere. Plumes of gas-saturated oil in the deep ocean (~1000 m) are highly confined due to weak currents at depth (Adcroft et al., 2010).

Attempts to understand the mechanism of methane release from marine sources has included physical observations, as well as physical and mathematical modeling of methane gas plumes. Physical observations have included the study of high methane fluxes in Black Sea (Bohrmann et al., 2003). Physical modeling of rising methane bubbles within and above the hydrate stability zone was conducted using deep-sea ROV (Rehder et al., 2002). Rehder et al. (2002) released methane and argon bubbles within the hydrate stability zone and witnessed reduced mass transfer rates supporting a commonly accepted assumption of hydrate rim

formation on methane bubbles rising from the hydrate stability zone (Maini and Bishnoi, 1981). DeepSpill was an experimental field study to simulate a subsurface oil and gas blowout at 844 m depth in the North Sea (Johansen et al., 2003). The DeepSpill experiment interestingly observed no hydrate formation despite thermodynamic conditions favoring hydrate formation. Later McGinnis et al. developed a single bubble model to explain vertical rise rate and dissolution dynamics (2006). However, the model developed by McGinnis et al. failed to predict the large amounts of methane escaping from the surface of the Deepwater Horizon spill. This discrepancy between the model and observation may lie in surface slicks of oil that transported methane in a dissolved (oil saturated) state.

In this work we quantify methane gas dissolution (from a liquid hydrocarbon carrier) behavior and rate using controlled *in situ* observations with methane saturated decane in the liquid phase. To address the questions regarding what quantity of methane is transferred to the mixed surface layer via hydrocarbon saturation, we use both laboratory and field approaches: In a series of controlled experiments aboard the RV *Rachel Carson* using the ROV *Ventana*, we simulated the dissolution of methane from a saturated oil and gas mixture of methane (CH<sub>4</sub>) and decane (C<sub>10</sub>H<sub>22</sub>). We utilized laser Raman spectroscopy to quantify the rate of dissolution of methane from decane.

Laser Raman spectroscopy is a type of vibrational spectroscopy capable of *in situ* molecular identification of solids, liquids, and gases. This optical technique is well suited to deep sea environments as it is a non-invasive, non-destructive and does not require consumables or sample collection (White 2009). An excitation laser hits a target, which is backscattered and collected by a sensor. Excitation radiation is focused on a small volume of material to create adequate power density, while permitting the spatial isolation of the scattered signal from that of background. Some of the backscattered spectrum is energy-shifted (Raman-shifted) such that the shifted radiation serves as a compositional and structural ‘fingerprint’ elucidating chemical species and phase (Ferraro et al., 2003). The backscattered photons may have lower (longer wavelength) or higher (shorter wavelength) energies (frequencies) than the excitation photons (Stokes and anti-Stokes scattering respectively). Backscattered spectrum is recorded as intensity (arbitrary unit [A.U.]) versus Raman shift (wavenumber [ $\Delta\text{cm}^{-1}$ ]) from the absolute frequency [ $\text{cm}^{-1}$ ] of the excitation radiation (Fig. 1).

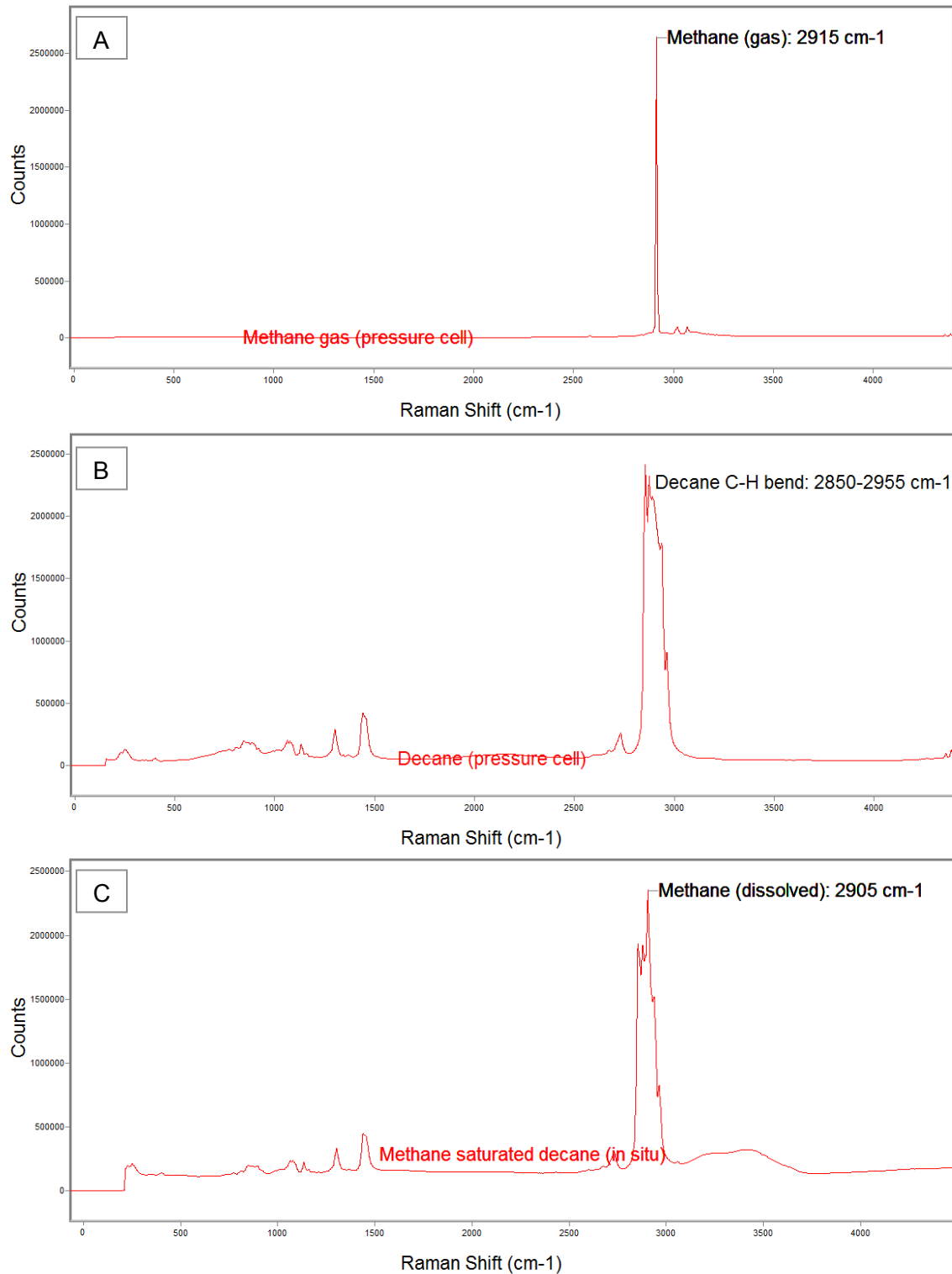


**Fig. 1.** Thermoscientific GRAMS/AI software spectral signatures of chemical species: (A) methane gas pressurized to 8.166 MPa (800 m depth equivalent), (B) decane at atmospheric pressure, and (C) methane saturated decane at 8.166 MPa pressure. Spectral signature is plotted as intensity counts [A.U.] vs. Raman shift in wavenumber [ $\Delta\text{cm}^{-1}$ ] shift from the absolute frequency [ $\text{cm}^{-1}$ ] of the excitation radiation. Characteristic spectral peaks include: methane ( $\text{CH}_4(\text{g})$ : 2915  $\text{cm}^{-1}$ ;  $\text{CH}_4(\text{l})$  2905  $\text{cm}^{-1}$ ) and decane ( $\text{C}_{10}\text{H}_{22}$ ; 2850-2955  $\text{cm}^{-1}$  C-H stretching complex).

## **MATERIALS AND METHODS**

### **RAMAN SPECTROMETER**

We analyzed lab-prepared samples of gas-saturated oils using the DORISS (Deep Ocean Raman In Situ Spectrometer) II system developed by Kaiser Optical Systems, Inc. (KOSI) and the Brewer Group at MBARI (Brewer et al., 2004). The spectrometer core components include: a KOSI Raman RXN optical bench f/1.8i spectrometer, front-illuminated, cooled, 512 x 2048 CCD camera manufactured by Andor Technology; a KOSI Invictus 100 mW, 532 nm frequency-doubled Nd:YAG laser; holographically filtered probe head to remove Raman scattering generated by excitation fiber and reject Rayleigh scattered light; and a holographic duplex grating. The 532 nm (green) laser light is ideal for ocean applications because this wavelength corresponds to the transmission peak of seawater (White 2009). The laser light is split into two paths on the camera via a duplex grating allowing measurement of full spectral range (100 to 4000  $\Delta\text{cm}^{-1}$  with  $\sim 2 \Delta\text{cm}^{-1}$  resolution). Raman optical bench with laser output (100 mW at the source and  $\sim 55$  mW at the point of measurement) and CCD camera are contained in a pressure housing assembly. Spectrometer and laser were connected via four fiber optic cables (one excitation fiber: 62.5  $\mu\text{m}$  diameter; and one collection fiber: 100  $\mu\text{m}$  diameter, and two spare fibers). Bare glass fiber optic cables were contained inside silicon oil filled hose with braided steel exterior to avoid uneven pressure stresses that would microfracture the fiber optic glass, resulting in signal losses.

For field work DORISS II is carried in portable drawer that fits into ROV payload sled. Raman laser spectrometer has a Non-Contact Optic (NCO) probe contained in a titanium housing with a dome optic housing. Probe head was positioned to provide a working distance (depth-of-field) of 23–25 cm from the radial center of a vertically oriented open bottom glass tube. This was the optimal in-water distance from the dome surface where the laser was most focused (focal point) for optimal sample interrogation and data collection.

### **CALIBRATION PROTOCOL**

We used neon and tungsten lamps for wavelength and intensity calibrations respectively in lab prior to cruise. Laser wavelength was calibrated against 801  $\text{cm}^{-1}$  Raman line of cyclohexane. Calibration and sample spectra were recorded using KOSI's HoloGRAMS software incorporating dark spectrum subtraction, with wavelength and intensity corrections applied. Returned spectra were recorded by KOSI's HoloGRAMS software and saved in generic

spectrum (.spc) format. Several spectral files were collected at each depth to observe changes in Raman-shifted peak areas.

#### ROV FIELD EXPERIMENTS

Laboratory decane ( $C_{10}H_{22}$ ) was pressurized with methane gas ( $CH_4$ ) prior to cruises and stored in a 4 L hydraulic piston accumulator with a zero pressure differential free sliding piston. Initial absolute partial pressure of methane in decane was 8.166 MPa. This partial pressure was calculated using Infochem MultiFlash software to mimic full saturation pressure at 800 m water depth where the ROV vertical ascent began. The accumulator was oriented such that its long axis was vertical with saturated oil in lower partition and pressurized water in upper partition controlled by a Seabird water pump (Fig. 2). Applying water pressure with the water pump into the seawater partition dispensed the methane/decane mixture into the glass tube. The dispensing outlet of the accumulator was equipped with a hydraulically-operated on-off valve to prevent uncontrolled dispensing due to pressure fluctuations.

Experimental cruises were performed aboard MBARI's RV *Rachel Carson* on July 1 and 2, 2013 in preparation for cruise aboard MBARI RV *Western Flyer*, September 5–10, 2013. The Raman spectrometer was mounted in tool sled of ROV *Ventana*. The ROV swing arm was mounted with an open bottom glass tube used for sample observation. The glass tube was attached to the swing arm via a hydraulic pump coupled with a linear bearing to manipulate the cylinder along its vertical axis to allow the Raman laser focal point to observe different phases of the methane/decane mixture (Fig. 3).

The methane/decane mixture was dispensed into the cylinder in discrete aliquots of ~90 mL for the three depth transect experiments. The methane/decane mixture was allowed to equilibrate to temperature of surrounding seawater at initial experimental depth of 800 m. The glass tube was observed with HD video during the experiments. During the static equilibrium experiment, Raman spectra were taken at five depths (600, 400, 300, 200, 100 m) during ascent of the ROV from 800 to 100 m. Two nonstop ascent experiments took spectra continuously during ROV ascent from 800 to 100 m.

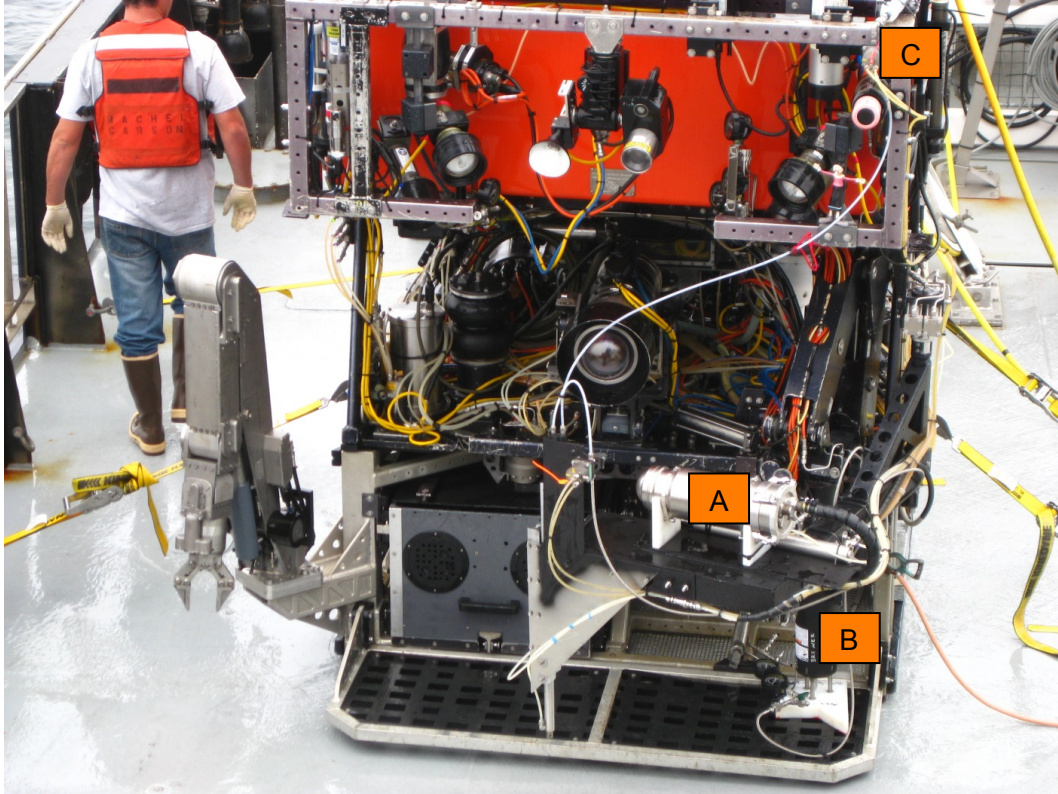


**Fig. 2.** Sampling hardware mounted on ROV including swing arm assembly with Laser Raman spectrometer (DORISS II; A), pressure accumulator (B), and Seabird water pump (C).

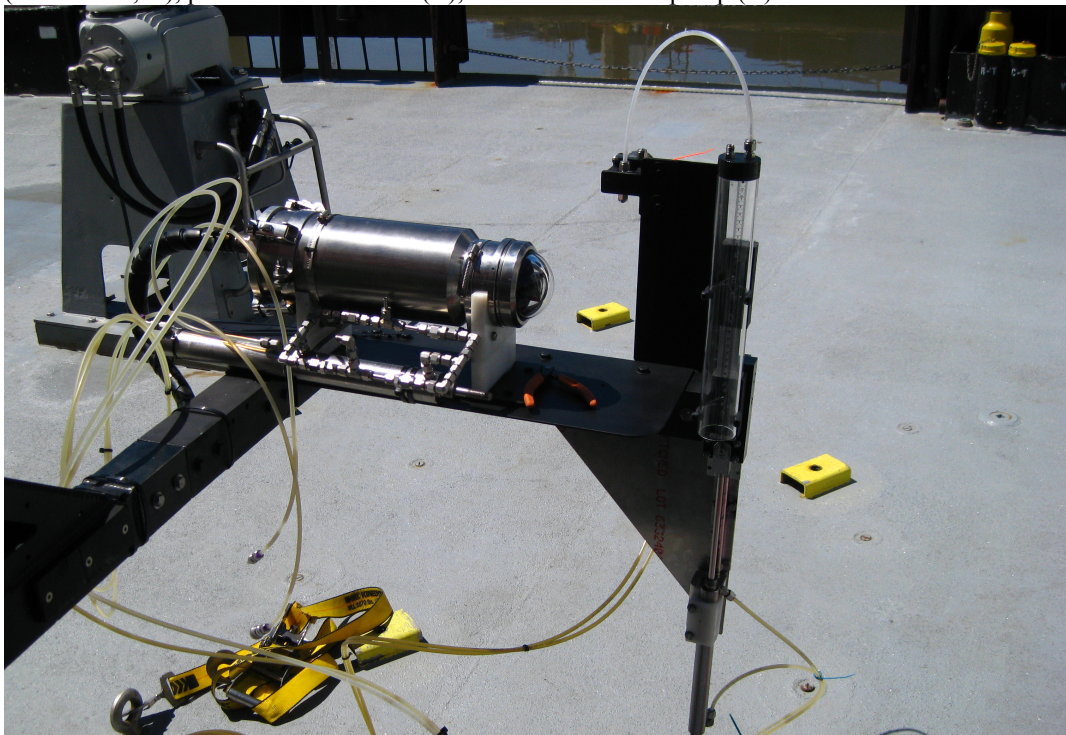


**Fig. 3.** The ROV swing arm assembly with laser Raman spectrometer positioned such that its focal point was positioned at the radial center of the glass tube. The glass tube was attached to the swing arm via a hydraulic pump coupled with a linear bearing to manipulate the cylinder along its vertical axis to allow the laser Raman to observe different phases of the methane/decane mixture.

## PRESSURE CELL REFERENCES

*In situ* samples of methane-saturated decane were compared to reference decane oil (without saturated methane) at same temperature and pressure conditions recorded during *in situ* ROV sampling. Reference spectra were taken using DORISS I (first generation laser Raman produced by the Brewer group) and the MBARI High Pressure-Low Temperature Raman Cell manufactured by Sam O. Colcate, Inc. (Fig. 4). Compressed air was used to pressurize the decane reference and a Haake K10 water bath was used to simulate *in situ* temperature conditions.

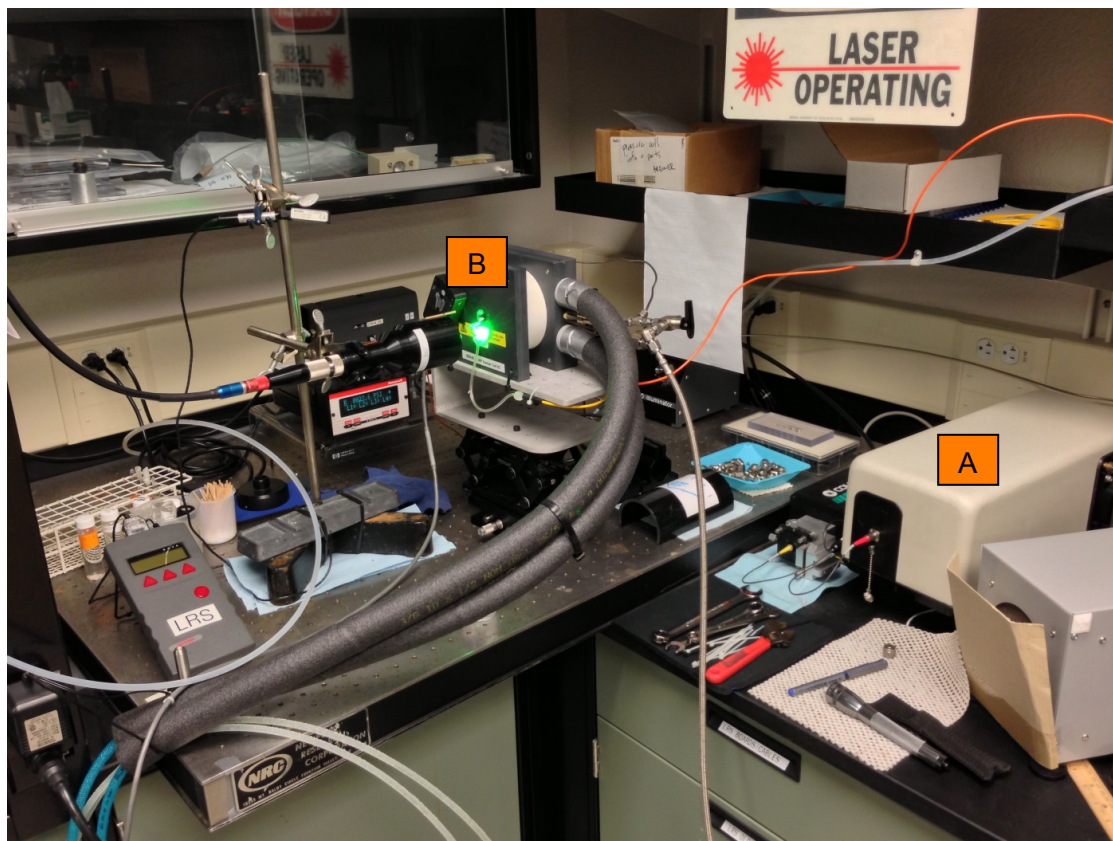


**Fig. 4.** Laboratory set-up for lab pressure cell experiments included DORISS I (A), the MBARI High Pressure-Low Temperature Raman Cell manufactured by Sam O. Colcate, Inc. (B), and a Haake K10 water bath (out of view).

## SPECTRAL ANALYSIS PROTOCOL

Given that Raman peak intensity is directly proportional to the concentration of the species in the sample (Dunk et al., 2005), we can use spectral peak area integration as a proxy for relative concentration. Methane and decane are strong Raman scatterers; however, distinctive peaks of the two species overlap where the methane peak is within the decane C-H stretching complex. For initial analysis, we plotted Raman spectra using Thermo Electron Corp.

GRAMS/AI software (Fig. 1). Later we deconvoluted the overlapping spectral signals of the two focal chemical species using a novel MATLAB protocol to perform a manual baseline correction centered on the C-H stretching complex (2780–3040  $\Delta\text{cm}^{-1}$ ) of both the *in situ* sample of methane saturated decane and a reference of pure decane (without saturated methane).

The reference spectra were then scaled using a scaling factor based on a ratio of max peak heights (A.U) within the C-H stretching complex of the sample and reference. Peak area integration of the C-H stretching complex (2780–3040  $\Delta\text{cm}^{-1}$ ) was committed for both sample and reference. Then peak area subtraction (Sample – Reference) yielded the difference spectra. Methane peak area was isolated by narrowing area of integration to Raman shift from 2895 to 2917  $\text{cm}^{-1}$  (Fig. 5). This protocol was repeated for all collected spectra. This novel spectral processing procedure was committed on multiple spectra at the five discrete depths of the static equilibrium experiment. Methane peak areas and peak heights were exported to spreadsheet software for analysis.

## **RESULTS and DISCUSSION**

### **ROV NONSTOP ASCENT EXPERIMENTS**

Two nonstop ascent experiments took spectra continuously during ROV ascent from 800 to 100 m. These spectral signals were then analyzed using MATLAB software to integrate the methane peak area within the C-H stretching complex. These area integrations were plotted versus time where experiment commences at 800 m depth and ascends to 100 m (Fig. 6). Using methane peak area versus time can yield general trends through time; however, this method is insufficient to quantify methane loss rate. Fig. 6 shows methane area increasing at the onset of the experiment. This increase in area would signify an increase in relative concentration of methane at the onset of the experiment, but thermodynamically, we know that methane can only decrease upon ascent given that pressure is decreasing and temperature increasing as the ROV ascends. Rising methane saturated decane becomes supersaturated with methane as it ascends the water column resulting in methane dissolution, not uptake. For a more complete understanding of methane loss rate, we must observe methane dissolution reaching equilibrium at static depths. Static depth allows ROV-recorded parameters (pressure and temperature) to be replicated in a laboratory setting.

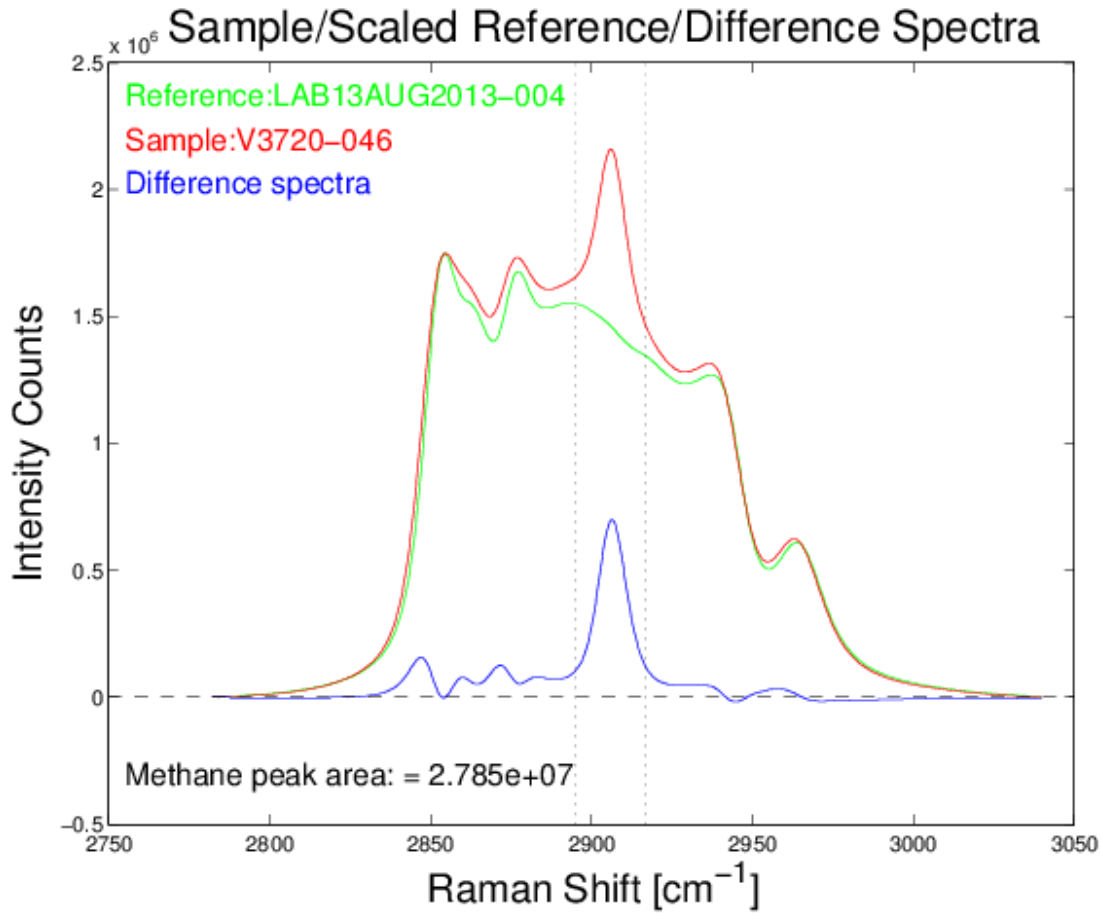


**Fig. 5.** Peak deconvolution procedure using MATLAB software. *In situ* samples taken aboard the ROV (red) were compared with pressure cell references (green) under same pressure and temperature conditions. After completing baseline subtraction (horizontal dotted line) on sample and reference, a scaling factor is applied to the reference to attain same peak intensities between sample and reference. Then peak area integration of the C-H stretching complex of both sample and reference is committed. Peak areas are subtracted to obtain a difference spectra (blue). Methane peak area is found by narrowing area of integration to Raman shift from 2895 to 2917  $\text{cm}^{-1}$  (vertical dotted lines).

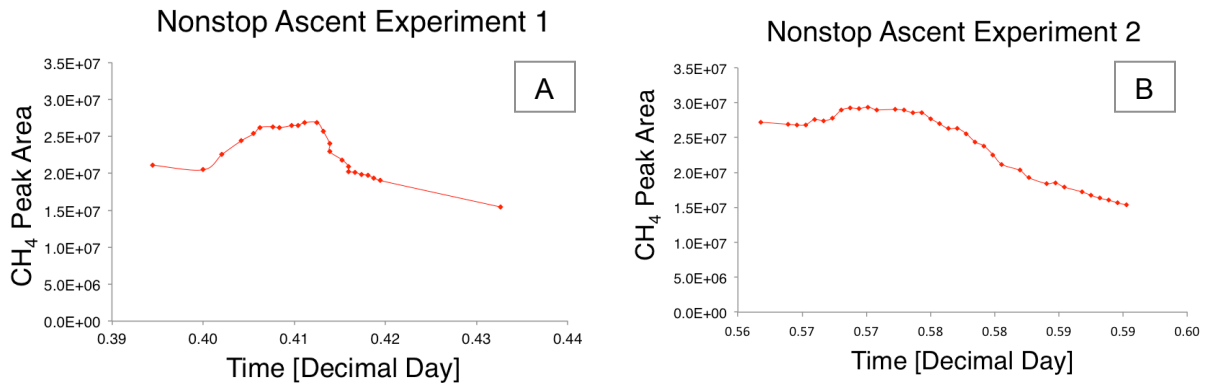


**Fig. 6.** Methane peak area plotted versus time (decimal day) for two rapid ascent experiments (A; B).

## ROV STATIC EQUILIBRIUM EXPERIMENTS

At five discrete depths (600, 400, 300, 200, 100 m), we collected spectra using the laser Raman spectrometer. Later in the laboratory, we then used a pressure cell to replicate the pressure and temperature conditions of the five discrete depths to take spectra of pure decane (no saturated methane). We then used the previously described deconvolution method to isolate the methane peak area using MATLAB. This method reveals relative changes in methane concentration. We determined absolute methane concentration from methane peak area and peak height of the ROV sample and pressure cell reference using Eq. 1:

$$Concentration(CH_4) = \frac{\left( \frac{Area(CH_4)}{Peak\ height(C_{10}H_{22})} \right)_{sample}}{\left( \frac{Area(CH_4)}{Peak\ height(C_{10}H_{22})} \right)_{pressure\ cell}} \quad (1)$$

Methane loss rate was determined using a linear regression of methane concentration changes versus time (Fig. 7). The slope of the linear regression of methane peak area versus time is the methane loss rate for a given depth. Methane loss rate was calculated to be 79.5, 476.6, 361.8, 327.2, 362.2  $\mu\text{M/s}$  at 600, 400, 300, 200, 100 m respectively. Linear regressions at all depths have a R value  $> 0.9$  (0.980, 600 m; 0.998, 400 m; 0.996, 300 m; 0.996, 200 m; 0.991, 100 m). We then compared methane loss rate with variables that may correlate with the observed changes in rate including depth, temperature, and pressure (Table 1). This comparison yielded no clear relationship between methane loss rate and any one variable of depth, temperature or pressure. The interface area between the methane saturated decane mixture and the evolved methane gas headspace above allowed a calculation of diffusion constant. We calculated a diffusion constant of 4.3, 25.9, 19.6, 17.8, 19.7  $\mu\text{M/cm}^2 \cdot \text{s}$  at 600, 400, 300, 200, 100 m respectively (Table 1). The diffusion constant at discrete depths varied due to changing temperature and pressure conditions in the water column. It is important to note that at 100 m depth bubble nucleation was contributing to methane loss rate in addition to diffusion across the interface. However, bubble nucleation did not reduce methane diffusion across the gas-liquid interface.

**Table 1.** Observed methane loss rate and diffusion constant at discrete depths during static equilibrium experiments.

Depth (m)	Absolute pressure (MPa)	Temp ( $^{\circ}\text{C}$ )	Methane dissolution rate ( $\mu\text{M/s}$ )	Diffusion constant ( $\mu\text{M/cm}^2 \cdot \text{s}$ )
600	6.145	5.89	79.5	4.3
400	4.114	6.93	476.6	25.9
300	3.103	7.66	361.8	19.6
200	2.089	8.29	327.2	17.8
100	1.083	8.87	362.2	19.7

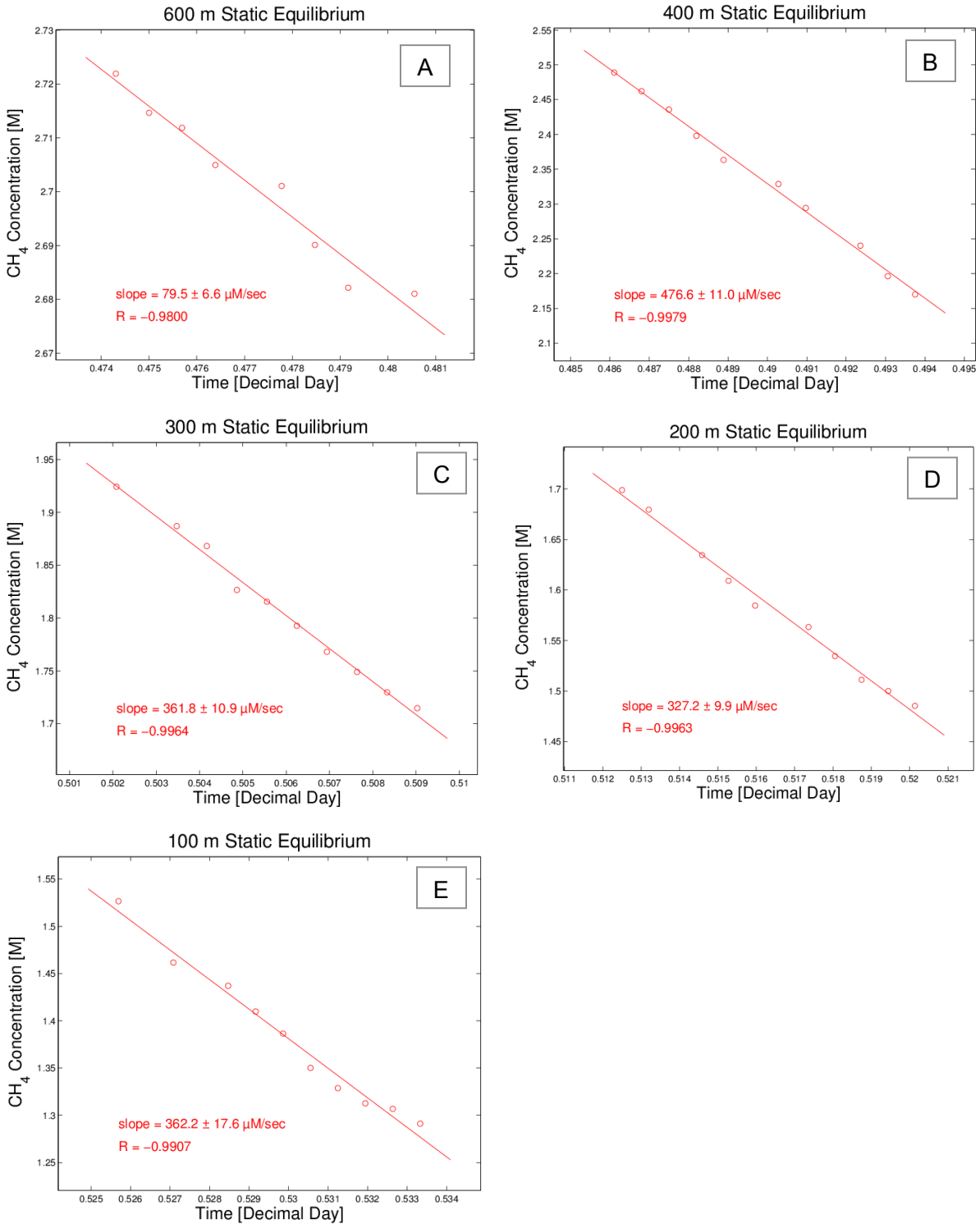


**Fig. 7.** Methane loss rates (slope of linear regression) for static equilibrium experiments for five discrete water depths: (A) 600 m; (B) 400 m; (C) 300 m; (D) 200 m; (E) 100 m.

## PRESSURE CELL EXPERIMENTS

Pressure cell experiments served as a reference of decane (without saturated methane) at the same pressure and temperature conditions of spectral samples taken by the ROV. Pressure cell experiments also offered an opportunity to compare the laboratory DORISS I and the sea-going DORISS II as the two separate spectrometers were used in the lab and in the field respectively. We collected spectra of pure decane using both DORISS II at 0.5 m depth in the MBARI test tank and DORISS I at the same pressure and temperature conditions of the tank using the pressure cell and water bath. Then we used the pre-described method to calculate the methane peak area. This comparison demonstrated that there is minimal horizontal translation of the spectral curve; however, some of the peaks within the C-H stretching complex have inconsistent intensity between DORISS I and II (Fig. 8).

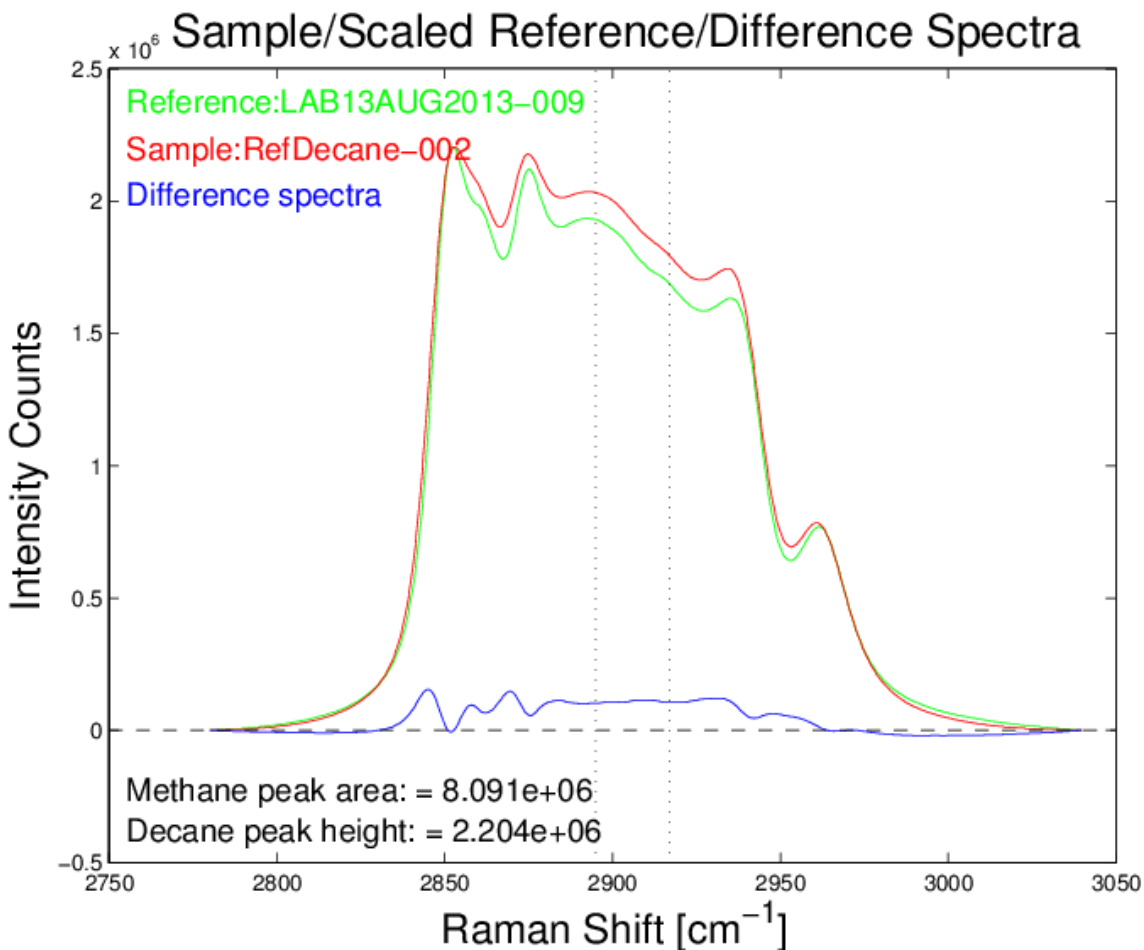


**Fig. 8.** Comparison of *in situ* derived samples (using sea-going DORISS II; red) to lab pressure cell samples (using DORISS I; green).

## CONCLUSIONS and RECOMMENDATIONS

Results from these *in situ* experiments demonstrate that rise rate of the hydrocarbon mass significantly exceeds the rate at which the excess dissolved methane may be lost by dissolution and bubble ebullition. The implication of this finding is that vertical transport of methane in the saturated hydrocarbon liquid phase may greatly exceed gas bubble ebullition ascending the water column from a seafloor source. Field work utilizing natural samples of gas saturated oils is needed to confirm such a proposition. Findings of this study increase the knowledge vertical distribution of methane above modern natural deep gas vents and anthropogenic oil and gas leakages from failed subsurface wellheads, pipelines, and risers. Furthermore, these results and observations contribute to an improved understanding of the composition, distribution, and environmental fate of leaked hydrocarbon mixtures and the vertical transport of carbon in the water column. This work will help to refine scenarios of future climate feedback associated with deep-sea methane releases.

## POST-EXPEDITION UPDATE

Laboratory pressure cell and field ROV dives were conducted in large part as preparatory experiments for study of natural oil and gas mixtures. These expedition experiments were conducted aboard MBARI's RV *Western Flyer*, on the 2013 Northern Expedition, September 5–10, 2013. Natural oils exhibit high level of fluorescence due to contained organic molecules. Fluorescence was observed when seeping oil droplets from the sea floor at the Eel River Canyon site fluoresced under the ROV lights. Similarly, when seeping natural oil was collected in a glass push-core, fluorescence inhibited any laser Raman spectral analysis of the oil (Fig. 9). After collecting the sample at 1800 m depth in a glass push core, ROV *Doc Ricketts* ascended, resulting in the dissolution of copious amounts of gas. The evolved gas from the sample of natural gas saturated oil was appropriate for Raman spectral analysis. In the evolved gas, we observed the following chemical species: methane (gas): 2915  $\text{cm}^{-1}$ ; ethane (gas) C-C region: 994  $\text{cm}^{-1}$ ; nitrogen (gas): 2330  $\text{cm}^{-1}$  among other dissolved chemical species (Fig. 10).

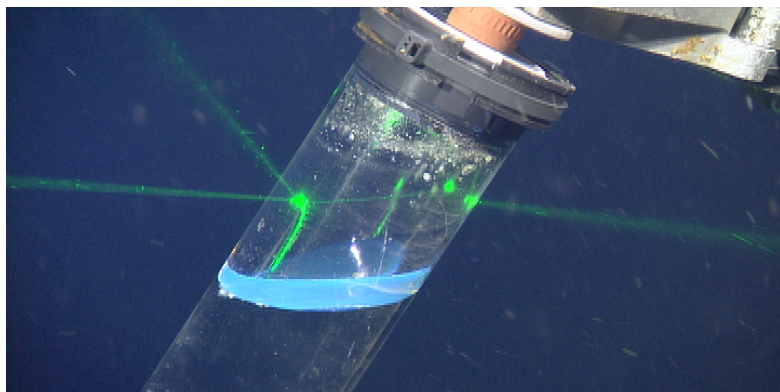


**Fig. 9.** Framegrab of gas saturated natural oil collected in a glass push core during the 2013 MBARI Northern Expedition aboard RV *Western Flyer*. Fluorescence inhibited laser Raman spectral analysis of the natural oil and gas mixture (blue layer). The evolved gas headspace, on the other hand, was appropriate for Raman analysis.

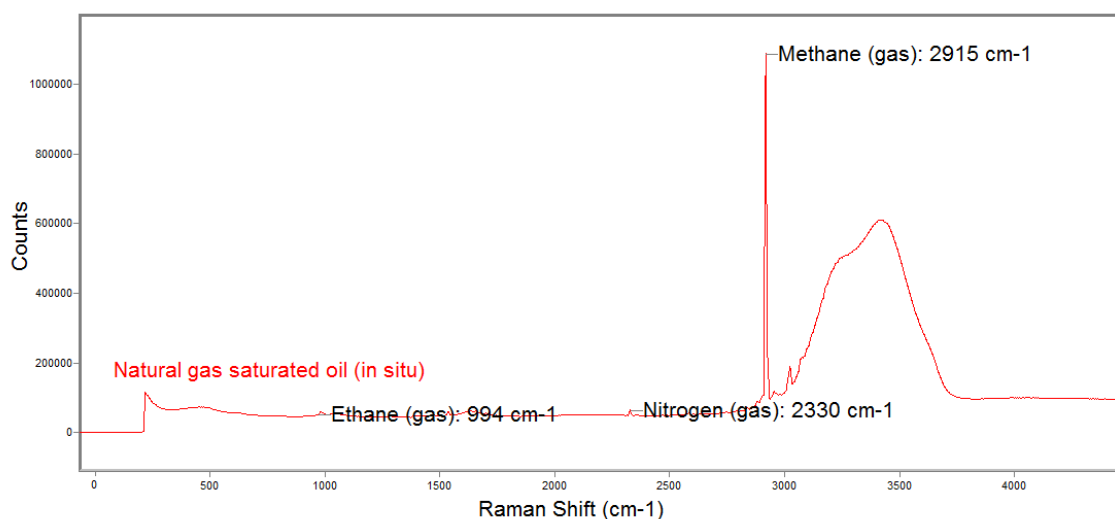


**Fig. 10.** Spectral curve of evolved gas from natural oil and gas mixture collected during the 2013 MBARI Northern Expedition including characteristic spectral peaks of methane (gas):  $2915\text{ cm}^{-1}$ ; ethane (gas) C-C region:  $994\text{ cm}^{-1}$ ; nitrogen (gas):  $2330\text{ cm}^{-1}$  among other hydrocarbon species.

## ACKNOWLEDGEMENTS

The 2013 MBARI Summer Internship Program was possible by the support of the David and Lucile Packard Foundation. Sincere thanks to the Brewer Lab including the mentorship of Peter Brewer, Edward Peltzer and Peter Walz. Special thanks to the officers and crew of the RV *Rachel Carson*, RV *Western Flyer* and ROV pilot teams of *Ventana* and *Doc Ricketts* for their expertise at sea. Many thanks to George Matsumoto and Linda Kuhn for MBARI internship program coordination. Thanks to intern colleague, Alba Cobo Viveros, for project support and assistance.

## REFERENCES

- Adcroft, A., R. Hallberg, J.P. Dunne, B.L. Samuels, J.A. Galt, C.H. Barker, and D. Payton (2010). Simulations of underwater plumes of dissolved oil in the Gulf of Mexico. *Geophysical Research Letters*, **37**: 5.
- Bohrmann, G., M. Ivanov, J.P. Foucher, V. Spiess, J. Bialas, J. Greinert, W. Weinrebe, F. Abegg, G. Aloisi, Y. Artemov, V. Blinova, M. Drews, F. Heidersdorf, A. Krabbenhöft, I. Klauke, S. Krastel, T. Leder, I. Polikarpov, M. Saburova, O. Schmale, R. Seifert, A. Alkenskaya, M. Zillmer (2003). Mud volcanoes and gas hydrates in the Black Sea: new data from Dvurechenskii and Odessa mud volcanoes. *Geo-Marine Letters*, **23**: 239–249.
- Brewer, P.G., G. Malby, J.D. Pasteris, S.N. White, E.T. Peltzer, B. Wopenka, J. Freeman, and M.O. Brown (2004). Development of a laser Raman spectrometer for deep-ocean science. *Deep-Sea Research Part I-Oceanographic Research Papers*, **51**: 739–753.
- Buffett, B. A. (2000). Clathrate hydrates. *Annual Review of Earth and Planetary Sciences*, **28**: 477–507.
- Crone, T.J., and M. Tolstoy (2010). Magnitude of the 2010 Gulf of Mexico oil leak. *Science*, **330**: 634–634.
- Cicerone, R.J., and R.S. Oremland (1988). Biogeochemical aspects of atmospheric methane. *Global Biogeochemical Cycles*, **2**: 299–327.
- Dando, P.R., P. Jensen, S.C.M. O'Hara, S.J. Niven, R. Schmaljohann, U. Schuster, and L.J. Taylor (1994). The effects of methane seepage at an intertidal/shallow subtidal site on the shore of the Kattegat, Vendsyssel, Denmark. *Bulletin of the Geological Society of Denmark*, **41**: 65–79.
- Ferraro, J.R., K. Nakamoto, and C.W. Brown (2003). *Introductory Raman Spectroscopy*. Academic Press, San Diego, CA.
- Herzberg, G. (1971). Spectra and structures of molecular ions. *Quarterly Reviews*, **25**: 201–222.
- IPCC (2007). Summary for Policymakers. In: *Climate Change 2007: The Physical Science Basis. Contribution of Working Group I to the Fourth Assessment Report of the Intergovernmental Panel on Climate Change* [Solomon, S., D. Qin, M. Manning, Z. Chen, M. Marquis, K.B. Averyt, M. Tignor and H.L. Miller (eds.)]. Cambridge University Press, Cambridge, United Kingdom and New York, NY, USA.
- Johansen, O., H. Rye, and C. Cooper (2003). DeepSpill - Field study of a simulated oil and gas blowout in deep water. *Spill Science & Technology Bulletin*, **8**: 433–443.

Kemsley, J. (2013). After the Deepwater Horizon disaster. *Chemical and Engineering News*, **91**: 12–17.

Kessler, J. D., D.L. Valentine, M.C. Redmond, M.R. Du, E.W. Chan, S.D. Mendes, E.W. Quiroz, C.J. Villanueva, S.S. Shusta, L.M. Werra, S.A. Yvon-Lewis, T.C. Weber (2011). A persistent oxygen anomaly reveals the fate of spilled methane in the deep Gulf of Mexico. *Science*, **331**: 312–315.

Leifer, I., R.K. Patro, and P. Bowyer (2000). A study on the temperature variation of rise velocity for large clean bubbles. *Journal of Atmospheric and Oceanic Technology*, **17**: 1392–1402.

Leifer, I., and R.K. Patro (2002). The bubble mechanism for methane transport from the shallow sea bed to the surface: A review and sensitivity study. *Continental Shelf Research*, **22**: 2409–2428.

Lelieveld, J., P.J. Crutzen, and F.J. Dentener (1998). Changing concentration, lifetime and climate forcing of atmospheric methane. *Tellus Series B-Chemical and Physical Meteorology*, **50**: 128–150.

McGinnis, D.F., J. Greinert, Y. Artemov, S.E. Beaubien, and A. Wuest (2006). Fate of rising methane bubbles in stratified waters: How much methane reaches the atmosphere? *Journal of Geophysical Research-Oceans*, **111**: 15.

McNutt, M. K., S. Chu, J. Lubchenco, T. Hunter, G. Dreyfus, S. A. Murawski, and D. M. Kennedy (2012). Applications of science and engineering to quantify and control the Deepwater Horizon oil spill. *Proceedings of the National Academy of Sciences of the United States of America*, **109**: 20222–20228.

Mezic, I., S. Loire, V.A. Fonoberov, and P. Hogan (2010). A new mixing diagnostic and Gulf Oil spill movement. *Science*, **330**: 486–489.

Milkov, A. V. (2004). Global estimates of hydrate-bound gas in marine sediments: how much is really out there? *Earth-Science Reviews*, **66**: 183–197.

National Research Council (2003). *Oil in the Sea III: Inputs, Fates, and Effects*, National Academic Press, Washington, D.C.

Maini, B.B., and P.R. Bishnoi (1981). Experimental investigation of hydrate formation behaviour of a natural gas bubble in a simulated deep sea environment. *Chemical Engineering Science*, **36**: 183–189.

Paris, C. B., M. Le Henaff, Z.M. Aman, A. Subramaniam, J. Helgers, D.P. Wang, V.H. Kourafalou, A. Srinivasan (2012). Evolution of the Macondo Well blowout: Simulating the

effects of the circulation and synthetic dispersants on the subsea oil transport. *Environmental Science & Technology*, **46**: 13293–13302.

Paull, C.K., W. Ussler, W.S. Borowski, and F.N. Spiess (1995). Methane-rich plumes on the Carolina continental rise - Associations with gas hydrates. *Geology*, **23**: 89–92.

Peltzer, E. T., and P. G. Brewer (2000). Practical physical chemistry and empirical predictions of methane hydrate stability, in *Natural Gas Hydrate in Oceanic and Permafrost Environments*, [M. D. Max (ed.)] Kluwer Academic Publishers, Dordrecht, 17–28.

Rehder, G., P.W. Brewer, E.T. Peltzer, and G. Friederich (2002). Enhanced lifetime of methane bubble streams within the deep ocean. *Geophysical Research Letters*, **29**: 4.

Ryerson, T.B., K.C. Aikin, W.M. Angevine, E.L. Atlas, D.R. Blake, C.A. Brock, F.C. Fehsenfeld, R.S. Gao, J.A. de Gouw, D.W. Fahey, J.S. Holloway, D.A. Lack, R.A. Lueb, S. Meinardi, A.M. Middlebrook, D.M. Murphy, J.A. Neuman, J.B. Nowak, D.D. Parrish, J. Peischl, A.E. Perring, I.B. Pollack, A.R. Ravishankara, J.M. Roberts, J.P. Schwarz, J.R. Spackman, H. Stark, C. Warneke, and L.A. Watts (2011). Atmospheric emissions from the Deepwater Horizon spill constrain air-water partitioning, hydrocarbon fate, and leak rate. *Geophysical Research Letters*, **38**: 6.

Vasconcelos, J.M.T., J.M.L. Rodrigues, S.C.P. Orvalho, S.S. Alves, R. L. Mendes, and A. Reis (2003). Effect of contaminants on mass transfer coefficients in bubble column and airlift contactors. *Chemical Engineering Science*, **58**: 1431–1440.

White, S. N. (2009). Laser Raman spectroscopy as a technique for identification of seafloor hydrothermal and cold seep minerals. *Chemical Geology*, **259**: 240–252.